Electronic Supplementary Material (ESI) for Reaction Chemistry & Engineering.
This journal is © The Royal Society of Chemistry 2024

Supporting Information

for

UiO(Zr)-based MOF Catalysts for Light-driven Aqueous Pollutant Degradation

Samuel C. Moore,[1] Isabella L. Hubble,[2] Alyssa L. Ritchie,[2] Jeffrey E. Barzach,[2] and Michele L. Sarazen[1,2]*

[1]*Department of Chemical and Biological Engineering, Princeton University, 41 Olden Street, Princeton, New Jersey 08544*

[2]*Department of Chemistry, Princeton University, Frick Chemistry Laboratory, Princeton, New Jersey 08544*

msarazen@princeton.edu

Table of Contents

Supporting Information

Structural Characterization

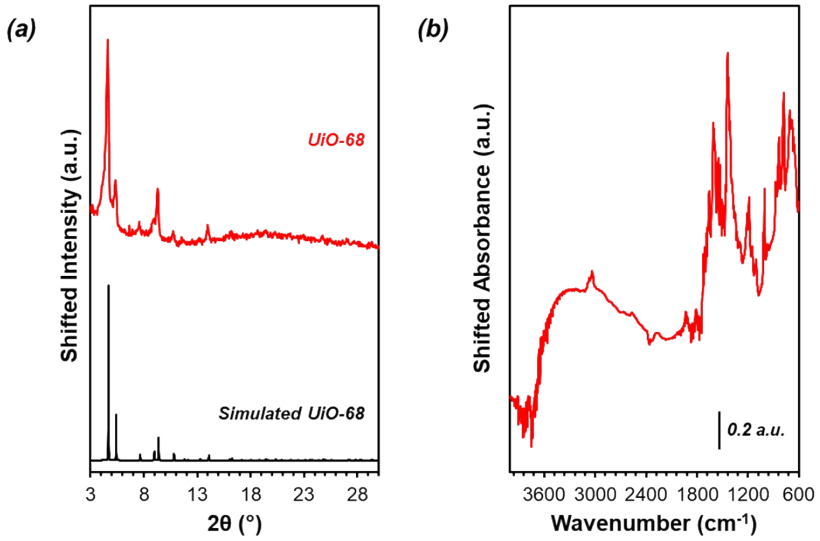

Figure S1. (a) UiO-68 experimental (red) and simulated (black) XRD patterns. (b) *Ex Situ* DRIFTS absorbance spectrum for UiO-68.

Diffuse-reflectance infrared Fourier-transform spectroscopy (DRIFTS) was performed on a Bruker INVENIO FTIR spectrometer equipped with a liquid N_2 cooled mercury-cadmium-telluride (MCT) detector and a Harrick Praying Mantis diffuse-reflection high-temperature reaction chamber equipped with two ZnSe windows. Observed bands are like those found in the UiO-67/Fe-UiO-67 MOFs and represent like functionalities. Bands at 1440 cm^{-1}, 1615 cm^{-1} and over the 2800-3600 cm^{-1} range are at similar frequencies to bands observed via FT-IR on UiO-67 as well as UiO-68 with linker functionalized on the central phenyl group by -NH_2, -F, -CH_3, and -OCH_3 groups, suggesting they are native to the triphenyl parent UiO-68.[1,2]

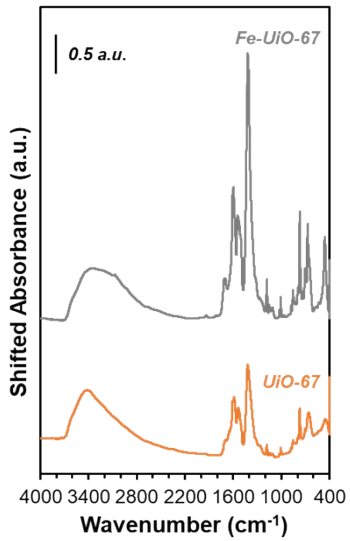

Figure S2. Extended *ex situ* FT-IR absorbance spectra for synthesized UiO-67 and Fe-UiO-67 (orange and gray, respectively).

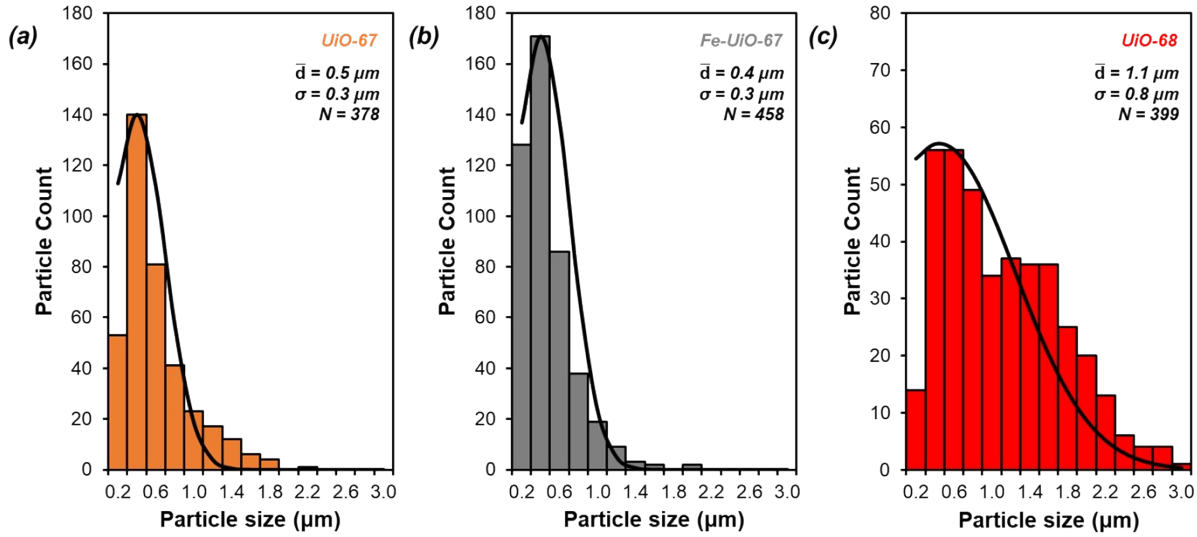

Figure S3. Particle size distributions for (a) UiO-67 (b) Fe-UiO-67 and (c) UiO-68 based on SEM images.

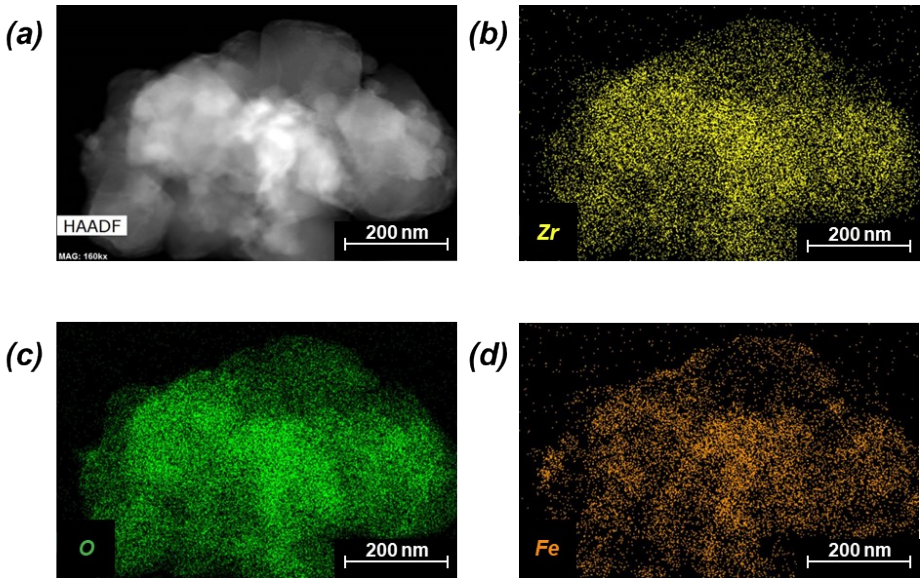

Figure S4. (a) STEM HAADF image of Fe-UiO-67 with accompanying EDX mapping of (b) Zr, (c) O, and (d) Fe elements (yellow, green, and orange, respectively).

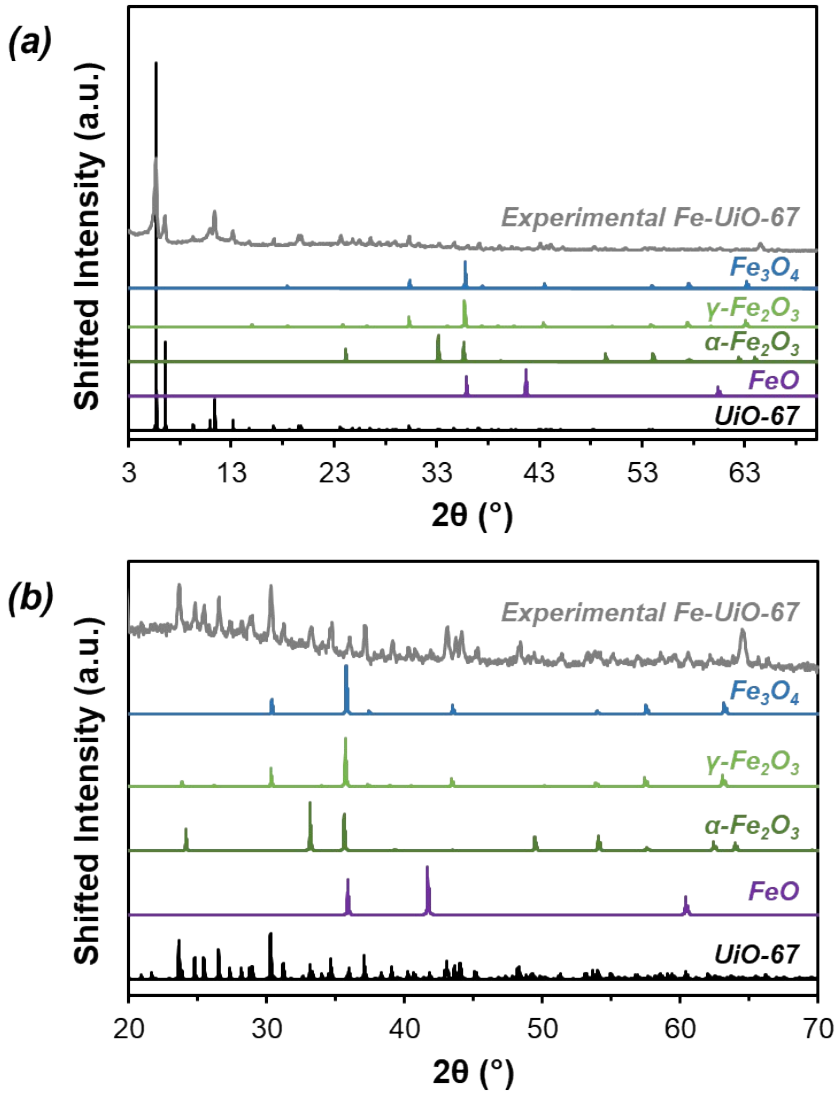

Figure S5. (a) Experimental Fe-UiO-67 (gray) and simulated UiO-67 (black), FeO (purple), α-Fe_2O_3 (dark green), γ-Fe_2O_3 (light green), and Fe_3O_4 (blue) XRD patterns.[3–7] Simulations are for defect-free crystals constructed using RIETAN-FP in VESTA.[8] Fe-UiO-67 intensity scaled up 2.5x. (b) Truncated and zoomed in experimental and simulated XRD patterns. Fe-UiO-67 intensity scaled up 3x and UiO-67 simulation scaled up 6x relative to presentation shown in (a).

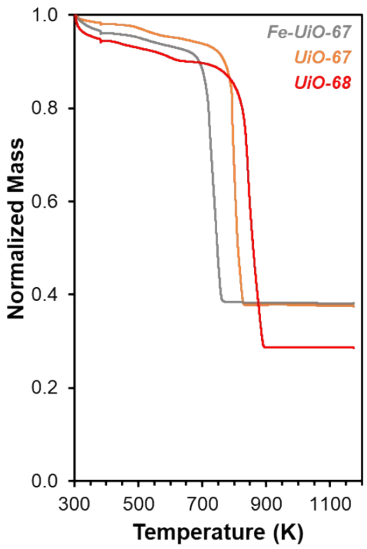

Figure S6. (a) Example normalized mass profiles obtained on TGA as function of temperature for UiO-67, UiO-68, and Fe-UiO-67 (orange, red, and gray, respectively, 383 K water bakeoff under argon followed by combustion in air up to 1173 K).

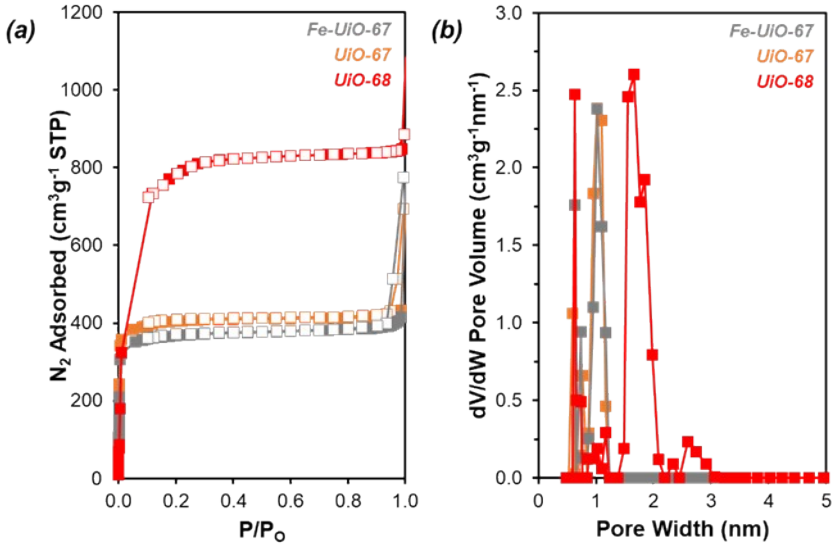

Figure S7. (a) N_2 physisorption isotherm (77 K, closed and open for adsorption and desorption, respectively) for Fe-UiO-67 (gray), UiO-67 (orange), and UiO-68 (red) with accompanying (b) NLDFT pore size distributions.

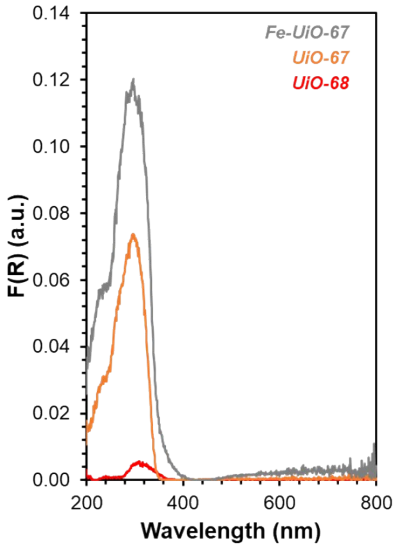

Figure S8. Diffuse reflectance spectra for Fe-UiO-67 (gray), UiO-67 (orange), and UiO-68 (red).

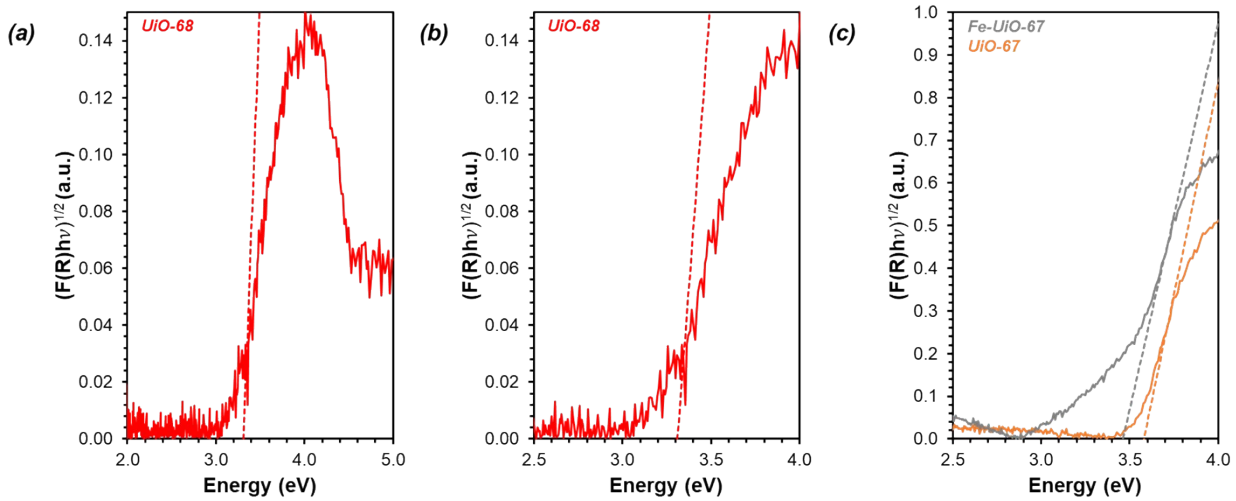

Figure S9. DR-UV-vis with K-M transformation applied for (a) UiO-68 (red), (b) a zoomed in section from the UiO-68 spectrum, and (c) a zoomed in section from the Fe-UiO-67 (gray) and UiO-67 (orange) spectra. Dashed lines represent tangent lines to the rise in absorption peak for BGE calculation.

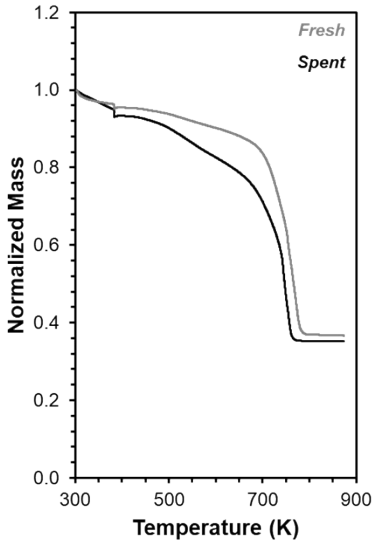

Figure S10. Normalized mass obtained on TGA as function of temperature for Fe-UiO-67 fresh and after being spent, solvent exchanged overnight in acetone, and dried at 343 K overnight (gray and black, respectively, 383 K water bakeoff in argon followed by combustion in air up to 873 K).

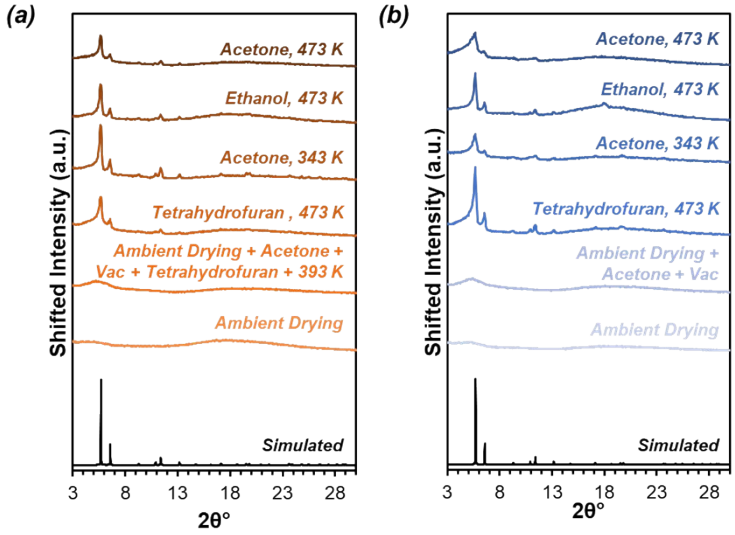

Figure S11. XRD patterns of UiO-67 heated to varied temperatures (ambient to 473 K) after exchanging with various organic solvents (none, acetone, ethanol, and tetrahydrofuran) (a) after exposure to MB, H_2O_2, and visible light in typical reactions and (b) after exposure to water alone under dark conditions.

MB Removal and Conversion

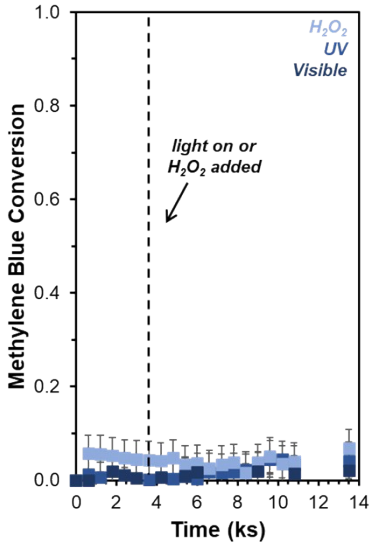

Figure S12. Temporal conversion profiles of MB in absence of UiO-MOFs (H_2O_2 only (light blue), UV light only (blue), visible light only (dark blue)) or of one another (initial charge of 0 g/L MOF, 0.031 mM MB, 0 or 4.0 mM H_2O_2, no light, 150 W Halogen lamp, or 370 nm UV lamp, 100 mL).

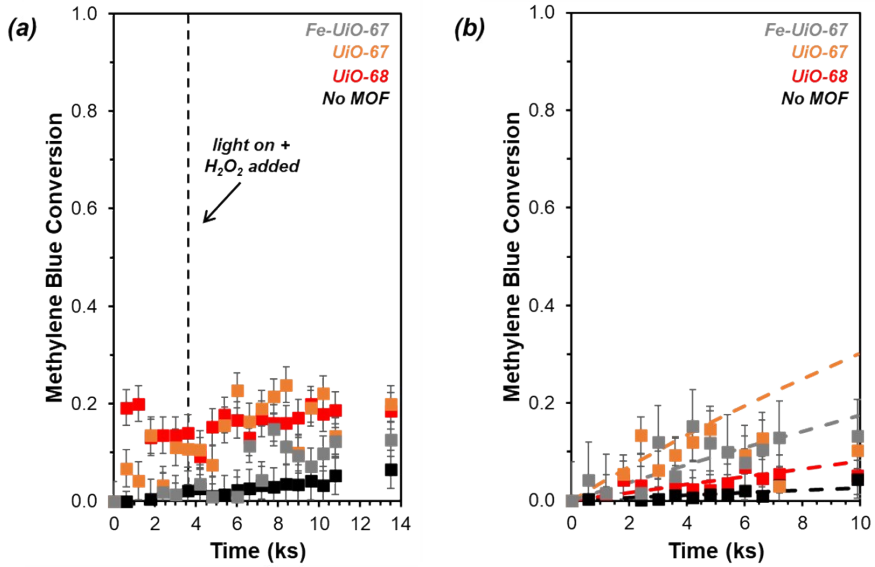

Figure S13. Temporal conversion profiles of MB with visible light activation and oxidant present (Fe-UiO-67 (gray), UiO-67 (orange), UiO-68 (red), no MOF (black)) (a) normalized to initial concentration and (b) renormalized to the bulk concentration remaining after a 3.6 ks period of interaction between the dye and MOF (initial charge of 0.25 g/L MOF, 0.031 mM MB, 4.0 mM H_2O_2, 150 W halogen lamp, 100 mL). Dashed lines represent modeled pseudo-first order kinetic profiles.

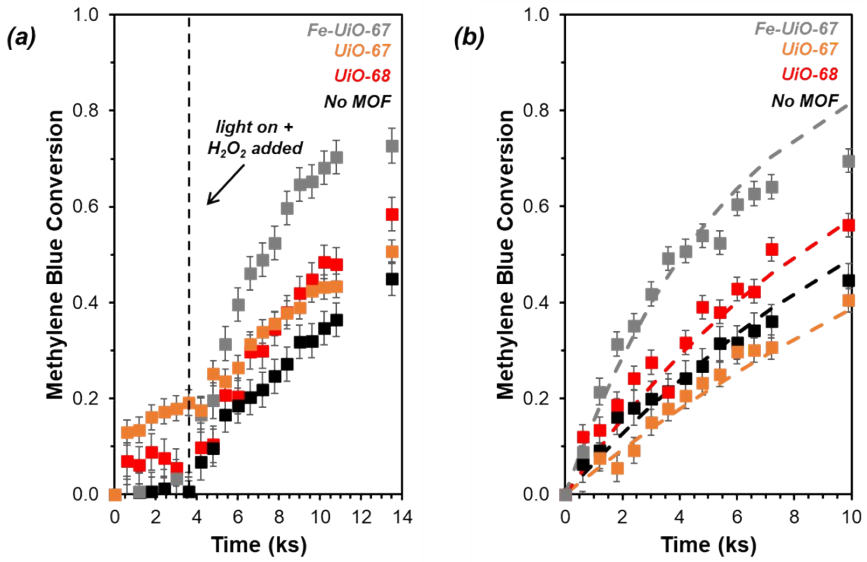

Figure S14. Temporal conversion profiles of MB with UV light activation and oxidant present (Fe-UiO-67 (gray), UiO-67 (orange), UiO-68 (red), no MOF (black)) (a) normalized to initial concentration and (b) renormalized to the bulk concentration remaining after a 3.6 ks period of interaction between the dye and MOF (initial charge of 0.25 g/L MOF, 0.031 mM MB, 4.0 mM H_2O_2, 370 nm UV lamp, 100 mL). Dashed lines represent modeled pseudo-first order kinetic profiles.

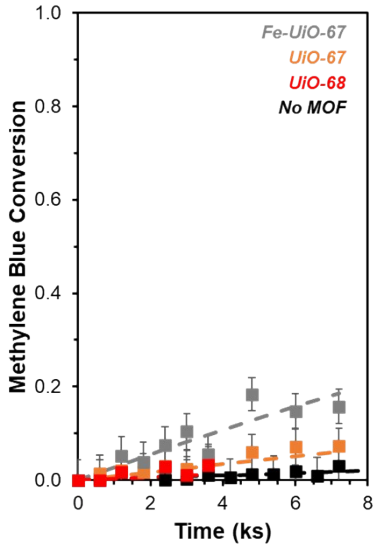

Figure S15. Temporal conversion profiles of MB with visible light activation and oxidant present (Fe-UiO-67 (gray), UiO-67 (orange), UiO-68 (red), no MOF (black)) in recovered supernatant fluid (0.0016 mmol MB added to 50 mL supernatant, 150 W halogen lamp).

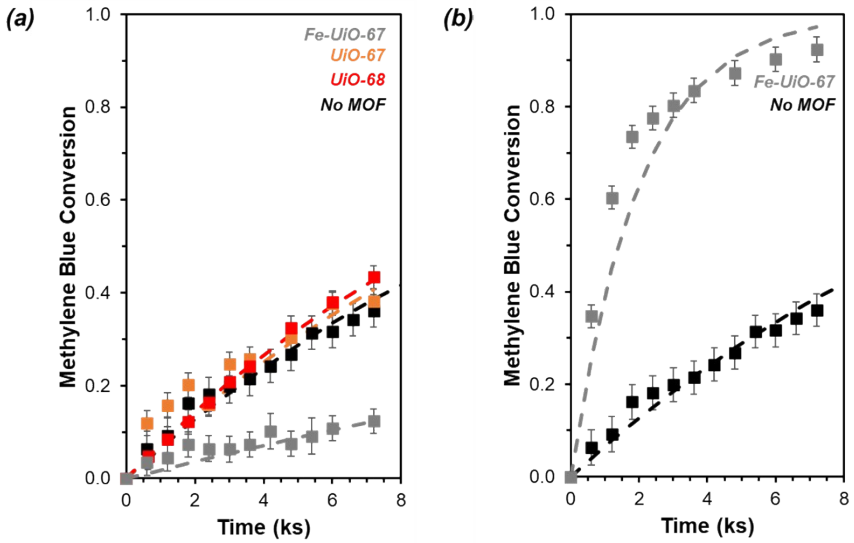

Figure S16. Extended temporal conversion profiles of MB with UV light activation and oxidant present (Fe-UiO-67 (gray), UiO-67 (orange), UiO-68 (red), no MOF (black)) (a) in recovered supernatant fluid with additional dye added (0.0016 mmol MB added to 50 mL supernatant, 370 nm UV lamp) and (b) with additional dye and oxidant added (0.0016 mmol MB and 0.19 mmol H_2O_2 added to 50 mL supernatant, 370 nm UV lamp). Dashed lines represent modeled pseudo-first order kinetic profiles.

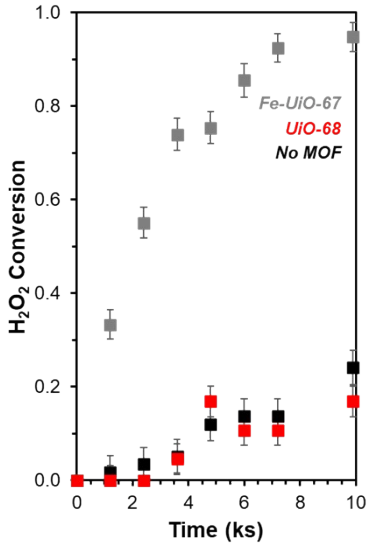

Figure S17. Temporal conversion profiles of H_2O_2 with UV light activation in the absence of MB (Fe-UiO-67 (gray), UiO-68 (red), no MOF (black)) (initial charge of 0.25 g/L MOF, 0 mM MB, 4.1 mM H_2O_2, 370 nm UV lamp, 50 mL)

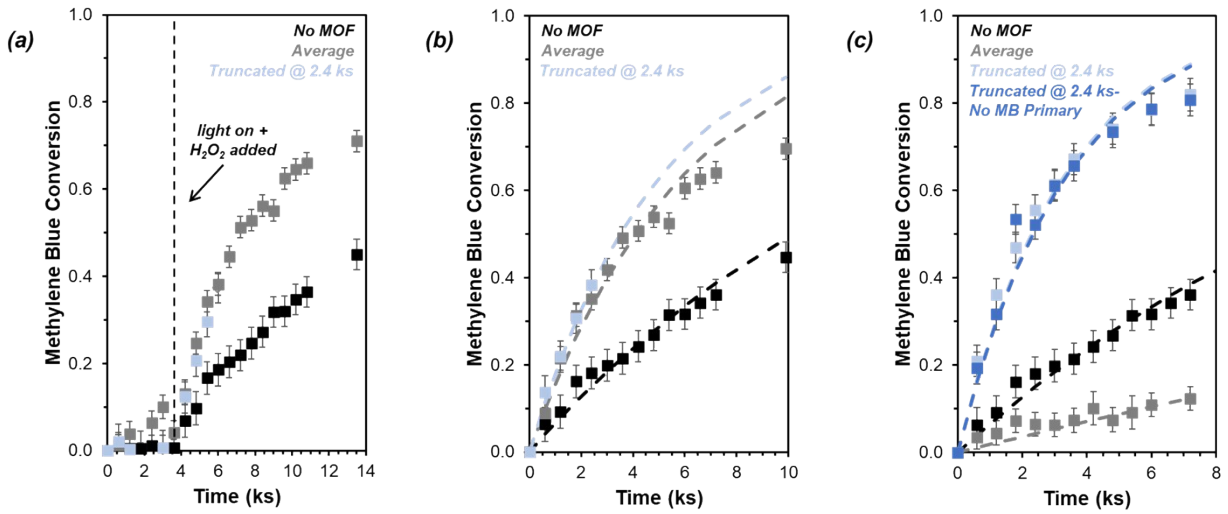

Figure S18. Temporal conversion profiles of MB with UV light activation and oxidant present (fresh, average Fe-UiO-67 (gray), Fe-UiO-67 truncated 2.4 ks after oxidant/light addition (light blue), no MOF (black)) (a) normalized to initial concentration and (b) renormalized to the bulk concentration remaining after a 3.6 ks period of interaction between the dye and MOF (initial charge of 0.25 g/L MOF, 0.031 mM MB, 4.0 mM H_2O_2, 370 nm UV lamp, 100 mL). (c) Temporal conversion in recovered supernatant fluid with additional dye added (0.0016 mmol MB added to 50 mL supernatant, 370 nm UV lamp). System in which no dye was added during H_2O_2 and UV exposure stopped at 2.4 ks (dark blue) include for comparison. Dashed lines represent modeled pseudo-first order kinetic profiles.

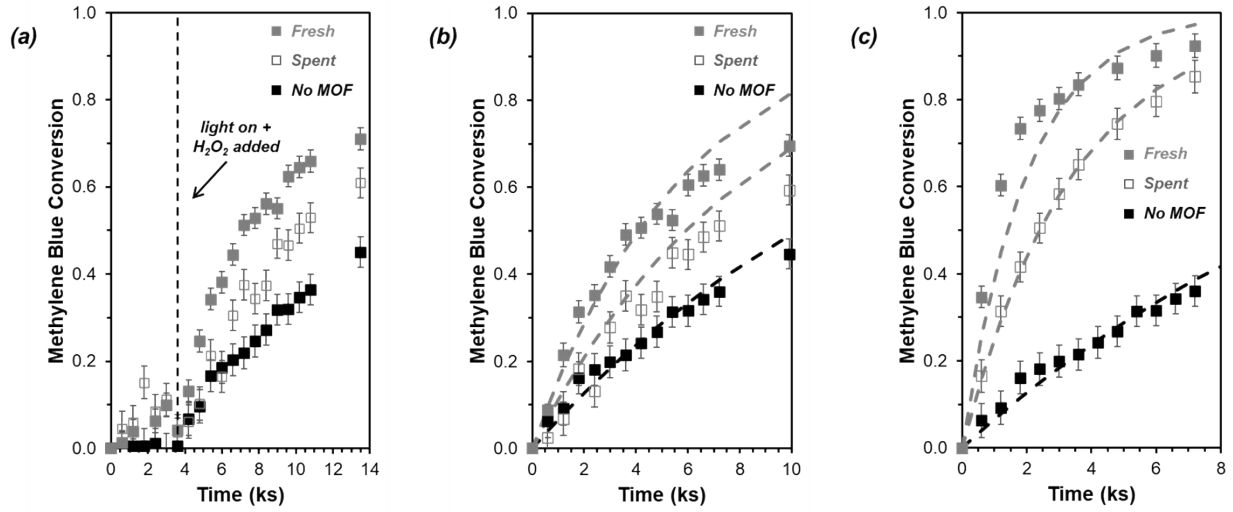

Figure S19. Temporal conversion profiles of MB with UV light activation and oxidant present (fresh Fe-UiO-67 (gray, closed), spent Fe-UiO-67 solvent exchanged with acetone and dried overnight at 343 K (gray, open), no MOF (black)) (a) normalized to initial concentration and (b) renormalized to the bulk concentration remaining after a 3.6 ks period of interaction between the dye and MOF (initial charge of 0.25 g/L MOF, 0.031 mM MB, 4.0 mM H_2O_2, 370 nm UV lamp, 100 mL for fresh and no MOF, 50 mL for spent). (c) Temporal conversion in recovered supernatant fluid with additional dye and H_2O_2 added (0.0016 mmol MB and 0.19 mmol H_2O_2 added to 50 mL supernatant, 370 nm UV lamp for fresh, 0.00095 mmol MB and 0.12 mmol H_2O_2 added to 30 mL supernatant, 370 nm UV lamp for spent). Dashed lines represent modeled pseudo-first order kinetic profiles.

Table S1. Pseudo-first order rate constants for visible-light activated condition (initial charge of 0.25 g/L MOF, 0.031 mM MB, 4.0 mM H_2O_2, 150 W halogen lamp, 100 mL).

MOF	Unnormalized k_{1st} (ks^{-1})	Mass-normalized k_{1st} ($g^{-1}ks^{-1}$)
None	0.003 ± 0.002	-
UiO-67	0.04 ± 0.01	1.4 ± 0.6
Fe-UiO-67	0.02 ± 0.01	0.8 ± 0.6
UiO-68	0.008 ± 0.006	0.3 ± 0.3

Weisz-Prater Criterion Calculations

Required effective diffusivities to achieve a kinetic regime of operation are determined based on the Weisz-Prater criterion for each MOF studied.[9] The limiting inequality defining a regime of kinetically limited operation is:

$$\frac{(r_v)_{obs}L^2}{D_e c_b} < 0.1$$

where $(r_v)_{obs}$ is the observed rate normalized by particle volume, L is the geometric parameter describing the catalyst particle (here the "radius", or half the length of the average crystal particle

obtained via SEM, approximating each particle as a sphere), D_e is the effective diffusivity of the component of interest (here, considered MB), and c_b is the concentration of that species in the bulk solution. Rearranging this inequality gives the minimum effective diffusivity in the catalyst required to achieve kinetically limited operation.

$$D_e > \frac{(r_v)_{obs} L^2}{(0.1) c_b}$$

The observed rate normalized by reaction volume is taken as the average degradation of MB over the first 3.6 ks after addition of H_2O_2 and UV light to the system (below). Catalyst density is required to relate catalyst mass addition to volume used; here it is based on the composition and spacing of atoms reported in perfect crystals.[7,10] Fe content present is assumed to have no impact on unit cell volume, only adding mass to the cell. Rates and density for each catalyst on this basis are calculated and reported below:

MOFs	Initial Rate ($mol \cdot L \cdot s^{-1}$) x 10^9	Density ($g \cdot cm^{-3}$)
UiO-67	0.8 ± 0.2	0.73
Fe-UiO-67	4.2 ± 0.2	0.78
UiO-68	1.4 ± 0.2	0.49

Based on the observed reaction rates at the typical reactant and catalyst concentrations studied, the minimum diffusivity required to achieve kinetically controlled operation is ~3 x 10^{-13} m^2/s for UiO-67 and ~7 x 10^{-13} m^2/s for both Fe-UiO-67 and UiO-68. Approximate effective diffusivities for MB in these structures is interpretable based on reported diffusivities of molecules of similar size or limitation reported in literature. One touchpoint for comparison is the aqueous diffusivity of terephthalic acid in UiO-66, reported to be 6.2 x 10^{-11} m^2/s, well above that required for the system to be kinetically controlled.[11] Although terephthalic acid is smaller, with molecular weight of 166 g/mol instead of 320 g/mol for MB, its calculated d_{vdW}, representing a surrogate for a kinetic diameter corresponding to the shortest cross-sectional ray incorporating the van der Waals radii of all atoms in the structure, is quite similar at 0.4 nm vs. 0.5 nm for MB. Moreover, UiO-66 is the smallest pore structure of the UiO family, with a pore limiting diameter of about 0.4-0.5 nm,[12,13] smaller than those of UiO-67 and UiO-68 at 0.6 nm and 1.0 nm, respectively.[13] Because each of these exceed the d_{vdW} of MB, they are expected to facilitate more facile transport of the molecule on size exclusion basis. Transport properties in Fe-UiO-67 are expected to be like those of UiO-67 given the minimal changes observed in surface area observed with N_2 physisorption.

Literature Cited

1 Y. P. Wei, Y. Liu, F. Guo, X. Y. Dao and W. Y. Sun, *Dalt. Trans.*, 2019, **48**, 8221–8226.
2 Y. Liu, Y. Zhao, Z. Zhou, Y. Shen and L. Jiang, *Colloids Surfaces A Physicochem. Eng. Asp.*, 2023, **674**, 131907.
3 E. R. Jette and F. Foote, *J. Chem. Phys.*, 1933, **36**, 29–36.
4 W. H. Bragg, *Nature*, 1915, **95**, 561.
5 L. Pauling and S. B. Hendricks, *J. Am. Chem. Soc.*, 1925, **47**, 781–790.
6 C. Pecharromán, T. González-Carreño and J. E. Iglesias, *Phys. Chem. Miner.*, 1995, **22**, 21–29.
7 S. Øien, D. Wragg, H. Reinsch, S. Svelle, S. Bordiga, C. Lamberti and K. P. Lillerud, *Cryst. Growth Des.*, 2014, **14**, 5370–5372.
8 K. Momma and F. Izumi, *J. Appl. Crystallogr.*, 2011, **44**, 1272–1276.
9 P. B. Weisz and C. D. Prater, *Adv. Catal.*, 1954, **6**, 143–196.
10 K. Manna, P. Ji, Z. Lin, F. X. Greene, A. Urban, N. C. Thacker and W. Lin, *Nat. Commun.*, 2016, **7**, 1–11.
11 A. Bigdeli, F. Khorasheh, S. Tourani, A. Khoshgard and H. H. Bidaroni, *J. Inorg. Organomet. Polym. Mater.*, 2020, **30**, 1643–1652.
12 M. J. Lennox and T. Düren, *J. Phys. Chem. C*, 2016, **120**, 18651–18658.
13 T. M. Al-Jadir and F. R. Siperstein, *Microporous Mesoporous Mater.*, 2018, **271**, 160–168.